# CHAPTER 6: NUMERICAL MODELLING OF THE SOIL

## 6.1 INTRODUCTION

This Chapter describes the formulation of two constitutive soil models and their application to the triaxial test, through single element modelling using spreadsheets to perform the calculations. The model adopted for the finite element formulation is explained and the application of this model to the axi-symmetric problem of a simple plate-loading test on sand is described. The material constants for the particular sand in this study and the model are presented.

## 6.2 SINGLE ELEMENT MODELLING

### 6.2.1 Introduction

A single element model was developed in a spreadsheet (Microsoft EXCEL) to calibrate material constants for subsequent finite element analysis, based on the agreement of the spreadsheet model predictions with the triaxial test data. Two variations of the soil constitutive model were developed, which differed in the treatment of the elastic response of the soil. The basic, or initial model, incorporated a constant Poisson's ratio and a Young's modulus varying with mean stress. The more sophisticated model required material constants for formulation of non-linear elastic behaviour, based largely on the work of Fahey and Carter (1993).

Three spreadsheet implementations of the single element model were developed to cover the different styles of triaxial tests that had been conducted. The theoretical basis of the basic model is given in Appendix C, while a flow chart representation for a conventional triaxial test is provided in Figure 6-1. Details of the refined model may be found in Appendix D.

### 6.2.2 Description of the Soil Constitutive Model

In the base model, the angle of friction, $\phi'$, varied with the level of stress and void ratio of the sand, and therefore, with the state parameter, $\xi$, of Been and Jefferies (1985). Inherently, the dilation rate as characterized by the dilation angle, $\Psi$, decreases as the state parameter increases, with the soil heading towards the critical state line from a state initially denser than critical state.

A simple yield criterion was adopted for demarcation between the elastic and the elasto-plastic phases of soil behaviour;

$$f = q - Mp' \qquad 6\text{-}1$$

where $p'$ = mean effective stress

and $q$ = the deviator stress, $\sigma_1 - \sigma_3$

However, the gradient of the peak strength failure envelope, M, is not constant but varies with $\phi'$, which in turn varies with the current value of the state parameter.

In the elastic phase, Young's modulus was assumed to be a function of effective mean stress as given by the power law;

$$E = mp_a \left[ \frac{p'}{p_a} \right]^{(1-a)} \qquad 6\text{-}2$$

Equation 6-2 is similar to Janbu's model (refer chapter 3, equation 3-2). As noted previously, Janbu's model used the minor effective principal stress as the variant rather than the effective mean stress. However his experiments were conducted in consolidometers, so mean stress varied directly with the minor principal stress. It would seem to be more acceptable to have moduli dependent upon mean stress for the wider range of potential stress sets that might be encountered in real applications.

In the proposed soil model, both bulk and shear moduli varied with the current effective mean stress, while Poisson's ratio was kept constant in the initial model.

Therefore the elastic response of the soil was dependent on the level of effective mean stress. It should be noted that as the sand was usually air dry, pore water pressure was not considered in any of the modelling.

#### 6.2.2.1 Implementation in a single element model in a spreadsheet

The model is simple to implement in a spreadsheet. In the three types of triaxial test considered here, axial strain is incremented, generating strains and stresses and hence the state parameter. Owing to the interdependence of the various parameters and the non-linear nature of the predicted behaviour, an incremental procedure is needed to solve the governing equations of the model. This measure does not cause significant error if step sizes are sufficiently small.

The effective mean stress is used to update the elastic stiffness matrix, which in turn is used to evaluate radial strain and subsequently update the effective mean stress, if the failure criterion has not been violated. With all stresses known, the state parameter, the mobilised effective angle of friction and the angle of dilation may all be determined. Therefore the elasto-plastic stiffness matrix is determinable. If failure of the soil has occurred ("f" becomes equal to zero), and then the elasto-plastic stiffness matrix replaces the elastic stiffness matrix.

"Consolidated Isotropically, then Drained" shearing (CID), or either constant mean stress or constant volume triaxial shearing conditions, are enforced easily in the numerical implementation. Details of the three implementations are provided in Appendix C.

### 6.2.3 Description of the Refined Model

The final or refined model adopted the Fahey and Carter (1993) approach to evaluating the current secant shear modulus, $G_s$, which requires the soil constants, f and g, in the plane strain formulation (refer Chapter 3):

$$\frac{G_s}{G_o} = 1 - f\left(\frac{\tau}{\tau_{max}}\right)^g \qquad 6\text{-}3$$

The small strain shear modulus, $G_o$, is a function of both void ratio and the current effective mean stress. The tangent shear modulus may be determined by differentiating equation 6-3.

An extension of equation 6-3 to three-dimensional stress conditions was made, based partly on Lee and Salgado (2000) (refer Appendix D for details). The resultant expression in terms of the tangent shear modulus was:

$$\frac{G_t}{G_o} = \frac{\left(G_s / G_o\right)^2}{\left[1 - f(1-g)\left(\frac{\sqrt{J_2} - \sqrt{J_{2o}}}{\sqrt{J_{2max}} - \sqrt{J_{2o}}}\right)^g\right]} \qquad 6\text{-}4$$

where, $J_2$ = $1/6\,[(\sigma'_1 - \sigma'_2)^2 + (\sigma'_2 - \sigma'_3)^2 + (\sigma'_1 - \sigma'_3)^2]$

$J_{2o}$ = the value of $J_2$ at the commencement of monotonic loading

$J_{2max}$ = the maximum value of $J_2$ attainable at the current effective mean stress, $p'$, corresponding to the failure criterion.

Following Naylor, Pande, Simpson and Tabb (1981) and Lee and Salgado (2000), it was assumed that the tangent bulk modulus, $K_t$, increased as a power law function of mean effective stress given by:

$$K_t = D_s (p')^{n_k} (p_a)^{(1-n_k)} \qquad 6\text{-}5$$

where $p_a$ = atmospheric pressure,

and $D_s$ and $n_k$ are material constants, with $n_k$ usually having a value of about 0.5 (e.g., Janbu 1963).

Equations 6-4 and 5 define the generalised forms of $K_t$ and $G_t$ to be incorporated into the elastic stress-strain law. Unlike the initial single element model, Poisson's ratio does not need to be specified as the elastic stiffness moduli, $G_t$ and $K_t$, are both separately formulated. At any stage, Poisson's ratio, $\nu_t$, may be deduced from the equation for isotropic elasticity from the expression:

$$\nu_t = \frac{3K_t - 2G_t}{6K_t + 2G_t} \qquad 6\text{-}6$$

In order to achieve realistic estimates of soil behaviour, it was found necessary to place a lower limit on $G_t$, which reduces with increasing deviator stress. If a limit is placed, the following condition must be satisfied:

$$\left(\frac{G_t}{G_o}\right) \geq r_g \qquad 6\text{-}7$$

where $r_g$ is a material parameter.

$r_g = 0$ corresponds to no limit on the reduction of $G_t$ with deviator stress

$r_g = 1$ corresponds to no reduction in $G_t$ with deviator stress, since $G_t$ is always less than $G_o$.

The refined non-linear "elastic" model described above was adopted in the single element model, which has been previously described.

### 6.2.4 Comparison between the Model Predictions and Test Data

#### 6.2.4.1 The basic model

The initial single element model's ability to predict the dilational behaviour of the sand in triaxial compression is illustrated in Figure 6-2. Strain increments of 0.0025 were applied throughout and were found to be a reasonable compromise between accuracy and practicality. A summary of the values of the material constants for the basic model is provided in Table 6-I. These values were derived in Chapter 5.

It is evident from Figure 6-2 that the model provided good simulation of dilational behaviour of the soil, although the onset of dilation was predicted to occur earlier than observed in the tests. As well, the predicted reduction of dilation at high levels of axial strain was not quite as quick as in the tests.

The stress-strain behaviour is broadly simulated by the single element model, as indicated in the plot of the conventional triaxial test, 53TRDAC, in Figure 6-3. This plot is typical of all other test simulations, which for purposes of clarity, have not

been presented. As the elastic modulus increases with mean stress, stiffness before yield is overestimated generally, then the stiffness sharply decreases as the soil softens during elasto-plastic deformation.

A comparison between the dilational behaviour in the constant mean stress tests and that predicted by the model is provided in Figure 6-4. As for the conventional triaxial tests, dilation is overstimated at high levels of strain. Since mean stress does not change, the elastic stiffness of the soil up to the point of yield is constant.

The simulations of the two "true" constant volume tests are provided in Figures 6-5 and 6-6. In the first of these Figures, the stress ratio, q/p′ has been plotted against axial strain, while in the second Figure, the deviator stress is shown as a function of strain. Test CVT1/95 was prepared to a density index of approximately 50%, while test specimen CVT2/95 was in a considerably looser state, having a density index of almost 30%.

When considering the stress ratio plot, it is evident that the soil behaviour is well modelled, within the limitations of the single element model, which were previously discussed. The model predicts the same behaviour for both specimens, regardless of their respective preparations.

However, when the variations of deviator stress with strain are considered, the simulation is found wanting in the case of test CVT1/95. The stress, q, is underestimated by approximately 35% as the axial strain increases above 2%. It would suggest that dilation will be underestimated in a constant volume test on a medium dense or denser specimen, taken to high levels of stress to contain volume change.

An alternative expression to Bolton's approximation for dilation was developed in Chapter 5 from the triaxial test series, which was attractive in its simplicity as it related dilation directly to state parameter, rather than indirectly, i.e.:

$$\Psi^\circ = -75\xi$$

This expression was trialled in the single element model, however it was found, as might have been expected, that there was no discernible difference in the predicted dilational response of the soil when compared with the single element model which included Bolton's approximation. Therefore Bolton's original expression was retained.

#### 6.2.4.2 The refined model

It became clear that the use of the refined non-linear elastic model achieved improved simulation of observed soil behaviour. The objective then became to find a set of material constants for the sand in the study that adequately represented the behaviour of all triaxial tests. Then these same values could be adopted with some confidence in the finite element model of more complicated boundary value problems, such as pipes buried in trenches and subjected to surface loading.

The selection of parameters was based on the degree of fit of the model predictions to the variation of stress ratio ($q/p'$) and volumetric strain with axial strain (%). Chosen values of the material constants are provided in Table 6-II.

The comparisons of the triaxial test data with the predictions from the refined model are provided in Figures 6-7 to 6-9 for the three sets of triaxial data. The comparisons are remarkably good for the majority of tests. The transition from elastic to elasto-plastic behaviour still remained relatively abrupt. Consequently, the peak stress tended to be overestimated.

Again the constant volume test CVT1/95 was not adequately modelled with respect to stress-strain behaviour. Deviator stress was again underestimated by more than 50% at high levels of axial strain. Nonetheless, the variation of stress ratio, $\eta$ (or $q/p'$), with axial strain was modelled well.

As previously discussed, both tests CVT1/95 and 2/95 were prepared in relatively loose states. There appears to be no plausible reason for the failure of the refined model to match the stress-strain data from CVT1/95. Unfortunately there was

inadequate time and material for a repeat of the test to verify the experimental results.

Given the excellent fit to the other test data, the refined model was considered to be an adequate representation of the non-linear, elastic and elasto-plastic stress-strain response of the sand used for the tests reported in this thesis.

## 6.3 THE FINITE ELEMENT MODEL FOR THE SOIL

The state parameter model was first implemented into the finite element program AFENA™ (Carter and Balaam 1995) by Dr. Peter Brown to assist his studies of screw plate testing in sands. Element type 44 was introduced and subsequently developed for generalised axi-symmetric finite element analyses of sand, which included torsional loading. The element provided an elasto-plastic, isotropic soil element with yield defined by the Mohr-Coulomb criteria.

Simple non-linearity in the elastic phase was possible, for example, through implementation of a model similar to that of Janbu's, which causes bulk and shear moduli to vary with the current effective mean stress (refer chapter 3, equation 3-2), while Poisson's ratio is kept constant. As noted previously, Janbu's model used the minor effective principal stress as the variant rather than the effective mean stress, although his test method constrained the mean stress to vary directly with the minor principal stress. It would seem to be more acceptable to have moduli dependent upon mean stress for the wider range of potential stress paths that might be encountered in real applications.

The first major development of element type 44 has been the implementation of the non-linear elastic behaviour embodied in the refined single element model, which was described in section 6.2.2. Therefore element type 44 now requires the eight material constants needed to define the non-linear elastic behaviour, namely, $D_s$, $n_k$, $C_g$, $e_g$, $n_g$, f, g and $r_g$. The reference atmospheric pressure must also be stated. To define the state line, material constants, $\lambda$ and $\Gamma$ are required. Intercept, $\Gamma$, is defined as the critical void ratio at a reference pressure of 1 kPa.

In order to evaluate the influence of state parameter on the current shear strength, the critical state friction angle, $\phi'_{cv}$, must be input, along with material constant, A, which relates the current value of the state parameter to the difference in effective friction angle, $(\phi' - \phi'_{cv})$ (refer equation 3-50). To estimate dilation from $(\phi' - \phi'_{cv})$, Bolton's factor is required. Bolton's factor is the coefficient in equation 3-26, which may be taken to be 0.8 or some other value.

As stated in Chapter 3, Bolton recommended that $(\phi' - \phi'_{cv})$ or $(\phi'_{max} - \phi'_{cv})$ was equal to $0.8\Psi$ for plane strain, although subsequently, numerous authors have applied the 0.8 factor for other strain conditions. As previously stated, the single element modelling of the triaxial tests showed this expression to be acceptable for simulation of triaxial test conditions, and so it was incorporated in element type 44.

The second major development has been the broadening of the model to three dimensional applications. Element type 43 was assembled in AFENA to deal with the three dimensional finite element analysis of buried pipes, as will be discussed in the following Chapter.

In order to minimize the analytical difficulties associated with soil tension developing in a purely frictional material, the state parameter element incorporated a tension cut-off, which corrected the effective mean stress back to zero, if a negative value was generated.

### 6.3.1 Comparison of AFENA element type 44 with the single element model

In order to verify the compilation of the element with the state parameter model, single element analyses of the conventional triaxial test were performed and compared with the single element results from the spreadsheet. An axi-symmetric analysis was conducted with a single 8-noded quadrilateral element representing a quarter of the triaxial specimen. The base of the element was fixed vertically, while nodes along the vertical axis of symmetry were fixed in the horizontal (or radial) direction.

A state of initial uniform stress was applied to the element corresponding to the constant confining pressure in the triaxial test. Deviatoric loading was applied by enforcing vertical (or axial) displacements along the top surface. Displacement increments were of similar size to the increments applied in the single element modelling. The quadrilateral element had nine Gauss points, from which, the deviatoric stress could be read at any stage in the analysis.

The comparisons between test data, the single element method (EXCEL) and the AFENA finite element analyses (FEA) are presented in Figure 6-10. The FEA predictions were identical to the EXCEL predictions in all respects but one; peak stress differed by less than 5%. AFENA provided slightly lower peak strengths; the program applies small corrections to the Mohr-Coulomb criterion to avoid the stress singularities and subsequent difficulties with stress integration, which can occur at low mean stresses and at the sharp corners of the Mohr-Coulomb failure envelope in the $\pi$ plane of stress space. The apex of the Mohr-Coulomb line was approximated with a hyperbola and the corners were rounded using circular arcs, in accordance with the recommendations of Abbo and Sloan (1995).

### 6.3.2 Application to the Plate Loading Test

As part of the buried pipe test series, the stiffness of the compacted sand was evaluated by a simple plate-loading test on the surface of the sand, the sand being contained within a cylindrical steel drum (see section 5.3). The diameter of the loading plate was 270 mm. The steel drum was 1.15 m high and had an internal diameter of 565 mm.

Two plate-loading tests were performed, with little difference between the load deflection behaviour evident between the two tests (refer Figure 5-4). Both tests were prepared to similar levels of density (average $I_D$ = 75%).

The soil was modelled with 440, 15-noded triangular elements, each element having twelve Gauss points. Only half the geometry of the drum needed to be modelled, because of vertical axial symmetry. The mesh is depicted in Figure 6-11. Boundary conditions are illustrated for a mesh with an interface joint between the sand and the steel drum. When either perfectly rough or perfectly smooth conditions were

adopted at the sidewall, the joint was removed and the appropriate boundary displacement conditions were applied. For the smooth wall condition, vertical fixity was applied along the base, while horizontal displacements were constrained on the vertical axis and along the side boundary. For the perfectly rough wall condition, the vertical displacement was additionally constrained at the side boundary.

An arbitrary average initial soil stress state was applied throughout the soil mass, consisting of 10 kPa vertically and 4 kPa horizontally. Prior to applying the external loading, equilibrium of the initial stress state was established.

Loading through the rigid plate was simulated by enforced displacements over the 21 surface nodes, extending from the centre of the mesh over a distance equal to the plate radius. The plate load at a particular displacement was determined by summation of the reactions of the nodes within the plate area.

Displacements were incremented slowly with usually 2000 equal-sized increments needed to reach 10 mm of plate displacement. These small size steps were found necessary to provide reasonable stability of the finite element analyses and, as will be shown later, there was little benefit in increasing the number of increments above 2000.

The stiffness matrix was updated after each increment, as the soil stiffness was dependent on the level of stress.

Two soil models were applied to analyse this case. Firstly the soil was treated as an isotropic and homogeneous, elasto-plastic material of constant shear strength and dilation angle ("Mohr-Coulomb" analyses). Secondly the soil was modelled with element type 44, which as explained in section 6.3 incorporated non-linear elastic behaviour (prior to yield) and the state parameter concept. Details of the two soil finite element analyses are provided in the proceeding sections.

#### 6.3.1.1 Mohr-Coulomb analyses

Yield was governed by the Mohr-Coulomb failure criterion, with non-associated plastic flow (dilation angle differs from the peak friction angle). The choice of

friction angle and dilation angle was based on the single element modelling of the conventional and constant effective mean stress triaxial tests, reported in Chapter 5. Four sets of soil strengths and dilations were adopted for the analyses (refer Table 6-III). The chosen values of peak friction angle were 30, 40, 45 and 50° and the corresponding dilation angles were 5, 10, 15 and 25°.

The Young's modulus of the soil was allowed to vary with effective mean stress according to equation 6-2 and employing the material constants for this equation given in Table 6-I, which were based on experimental data presented in Chapter 5.

Analyses with the Mohr-Coulomb element were attempted with both smooth and rough sidewalls. A sidewall joint was not considered. A tabulated summary of input for the Mohr-Coulomb analyses is provided in Table 6-III.

#### 6.3.1.2 State Parameter analyses

A range of density indices was assumed for the soil as indicated in Table 6-IV, namely 50, 75 and 85%. Density indices were converted to void ratios on the basis of the maximum and minimum void ratios for the sand, which were 0.893 and 0.520, respectively (refer Chapter 5).

The State Parameter material constants and deformation and strength constants that were applied in the model for the soil, are presented in Table 6-I.

Apart from two of the analyses, an elasto-plastic interface element or joint was introduced at the sidewall. A Goodman type joint was implemented, which required both the elastic shear and normal stiffnesses of the joint (in units of stress per unit of displacement), the effective angle of friction and the angle of dilation of the interface. The joint interface was assumed to be non-cohesive and dilation was ignored.

The values adopted for joint stiffness and strength, given in Table 6-V, were based on a series of direct shear box tests. The direct shear tests were conducted with plywood from the soil box placed in the bottom half of the box, and the sand tamped into position in the upper half of the shear box. The tests were performed to assess

the influence of sidewall friction of the shear box in the buried pipe tests. Although the steel of the drum and the plywood of the soil box are different materials, it was believed that the joint characteristics would not be significantly different, judging by friction studies on timber and steel piling in non-cohesive soil (Tomlinson 1975).

#### 6.3.1.3 Results of the finite element analyses

The Mohr-Coulomb finite element analyses were compared with the test data in Figures 6-12 and 6-13, the former Figure showing predictions (load-deflection for the plate) from analyses with a perfectly rough sidewall, the latter showing analyses with the same soil properties, but with a smooth sidewall. Very few analyses achieved the target displacement of 10 mm. Finite element analyses generally ended prematurely after the development of tension in Gauss points within elements beside the edge of the loading plate and near the soil surface.

Finite element analyses with a smooth sidewall were more successful in terms of the length of the analysis (simulating more plate displacement), however these analyses were less able to simulate the experimental data than the rough wall analyses. The modelled soil response was far less stiff than the observed load deflection response of the soil confined within the drum. To emphasise this point, the predictions from the analyses with rough and smooth sidewalls, MCr5025 and MCs5025 respectively, have been plotted together in Figure 6-14. The effective angles of friction and dilation were 50° and 25°, respectively in these analyses.

In reviewing Figures 6-12 and 6-13, it can be seen that as the strength and dilation of the sand were increased, the stiffness of the soil to the surface loading also increased. However, even after adopting a peak effective friction angle of 50° and dilation angle equal to the friction angle, as well as a rough sidewall, the experimental data could not be matched. The stiffness of the model was less than that of the sand as revealed in the plate load tests.

Mohr-Coulomb analyses could be made to work adequately by less judicious choice of parameters. The parameters chosen for the finite element analyses were derived from careful analyses of the triaxial tests on the sand and are therefore regarded as being rational. The fact that the implementation of these values has not resulted in a

satisfactory modelling of the plate load test in the sand drum suggests that the Mohr-Coulomb approach is inadequate.

The state parameter approach was more successful. The load-deflection plots for the three state parameter analyses in which the initial density varied, are provided in Figure 6-15 (analyses Saldrum 2, Saldrum1 and Saldrum3, corresponding to density indices of 50, 75 and 85% respectively). In these analyses, an interface joint was incorporated along the sidewall. All analyses were designed for a maximum surface displacement of 10 mm after 2000 increments.

It is apparent that a sand density index of 85% brought the finite element analysis in line with the experimental data. As the density index decreased, the modelled sand's response was less stiff. The density index determines the soil's initial void ratio and, with the effective mean stress, determines the state parameter, which impacts directly on the peak friction angle and dilation of the soil, as well as the soil stiffness.

The influence of the treatment of the sidewall on the plate load-deflection response is shown in Figure 6-16 for a soil density index of 85% (analyses Saldrum 3, Saldrum5 and Saldrum6, corresponding to jointed, smooth and rough wall conditions, respectively). As observed with the Mohr-Coulomb element analyses, a smooth sidewall resulted in a longer analysis (greater plate deflection before solution instability occurred) than was realised with a comparable FEA with a rough wall. The jointed wall analysis was also more successful than the rough wall analysis in terms of the plate deflection that was reached.

In the smooth wall analysis, it appeared that the soil was initially too deformable when compared with the test data, but became adequately stiffer with loading. Lack of shear support at the sidewall would undoubtedly allow easier plate deflection until the contained soil volume could offer greater resistance. Accordingly, the rough wall analysis produced a much stiffer soil response in the early stages of plate loading than the smooth wall analysis.

The jointed wall model resulted in a load-deflection curve that was slightly less stiff than the response of the rough wall analysis. For the same level of surface

deflection, the rough wall analysis generated between 10 and 20% more reaction or equivalent plate loading.

It may be concluded that a rough wall analysis could provide an adequate match to the test data, but would require a reduction in the initial density index (or strength) of the soil. Figure 6-17 provides predictions from further finite element analyses with a rough sidewall and initial sand density indices of 65, 75 and 85% (Saldrum8, Saldrum9 and Saldrum6, respectively). The agreement with the experimental data is clearly evident, but only in the early stages of the analysis, for the case with a density index of 65%.

Finally a check was performed on the number of displacement increments required to make a successful analysis, by repeating Saldrum3 with 1000 and 5000 increments (these analyses being entitled Saldrum7 and Saldrum8, respectively). It can be seen from the predictions reproduced in Figure 6-18 that FEA with 2000 increments is quite adequate. The differences between the loads estimated to reach a plate displacement of 3.9 mm relative to the 5000 increment run, were only -0.2 and -0.1 % for the 1000 and 2000 increments analyses, respectively.

Analyses were successful to 4.2, 4.0 and 3.9 mm of plate displacement, for 1000, 2000 and 5000 increments, respectively. The finite element analyses generally ended with the development of tension within interface joint elements near the top of the mesh at the side boundary.

Predictions from Saldrum3 ($I_D$ of sand, 85%, jointed wall and 2000 increments per 10 mm) are provided in the four Figures, 6-19 to 6-22. All the Figures contain data relevant to an enforced displacement of the loading plate of 4.0 mm. The first of these Figures shows contours of the vertical deflections of the sand mass. The contours are smooth and tend to emanate from the edge of the plate. Very little deformation was evident in the lower half of the mesh. In Figure 6-20 the vertical and horizontal deflections of the sand are presented as a deformed mesh, exaggerated by a factor of 5. An outline of the initial mesh has been overlaid. While the plate has pushed down the underlying sand surface uniformly by 4 mm, the adjacent sand has settled only by one millimetre.

The remaining two Figures provide mean effective stress contours and locations of yielded Gauss points in the top half of the mesh. Effective mean stress was greatest and was concentrated, as would be expected, in the two elements immediately below the plate edge, just where a stress singularity should occur. The maximum mean stress in this area was 184 kPa. At the same level of displacement, the vertical contact stress below the footing was an average of 182.6 kPa, based on the sum of the nodal reactions of the loaded nodes.

Stress gradients were high between the elements to either side of the plate edge at the surface of the soil. Away from the loaded area, the stress in the sand was low. Just below the soil surface and 2 mm either side of the edge of the plate, the mean effective stress varied from 184 to 36 kPa.

Locations of plastic Gauss points are shown in Figure 6-22. At 4 mm of plate displacement, yield had extended through an almost rectangular block of elements adjacent to the edge of the plate, two elements wide and seven elements deep (34 mm by 105 mm). The depth of this zone corresponded to approximately 0.4D, where D is the diameter of the plate. All surface elements outside the plate contained plastic Gauss points and yield had occurred in the elements along the sidewall within a block three elements deep (32 mm). Yield in this zone was anticipated, as the stress levels are low near a free surface.

## 6.4 SUMMARY OF THE CHAPTER

The application of a spreadsheet for single element modelling of triaxial test data has been shown to be a valuable exercise to develop constitutive models for soils. In this Chapter, an elasto-plastic, isotropic model incorporating the state parameter concept has been developed. Yield is defined by the Mohr-Coulomb criterion. Post-yield deformations are based on a non-associated flow rule defined by Bolton's findings and the state parameter concept of Been and Jeffries. The effective friction angle of the soil varies with the state parameter.

The refined single element model incorporated non-linear elasticity with both the shear and bulk modulus not directly linked. The non-linearity requires eight material constants. It was found that a set of material constants could be established which adequately modelled the majority of the triaxial tests on the sand used in this investigation of the performance of buried flexible pipes. The triaxial tests included three CID, five constant effective mean stress, and two constant volume tests. A further five material constants are required to implement the state parameter model.

Subsequently the model has been incorporated into finite element program AFENA. The single element analyses of the conventional triaxial tests were compared with comparable finite element analyses, which verified that the implementation of the model into program AFENA was successful.

The application of the State Parameter model has been demonstrated for the finite element analysis of a plate-loading test in the sand, confined within a drum. This geotechnical problem is difficult to model because of the sharp vertical stress change below and near the edge of the rigid loading plate ("singularity") and the likelihood of tension and plasticity near the unloaded soil surface.

It was shown that the state parameter model was superior to the Mohr-Coulomb approach, in which a constant effective angle of friction and angle of dilation are assumed. The state parameter model constantly updates values of both dilation and angle of friction based on the current effective stress and void ratio of the soil, i.e. based on the value of the state parameter.

The implementation of an interface joint along the sidewall improved the modelling of the plate load test with the state parameter, when compared with the assumption of a perfectly rough sidewall condition. In contrast, a perfectly smooth wall was found unable to adequately represent the test data.

The average density index of the soil in the plate loading tests was estimated to be 75%, however a density index of 85% was required in the finite element analyses to achieve the best match with the load-deflection test data. A possible conclusion is that the average density index inferred from dynamic penetration testing of the sand was underestimated. It should be noted that the influence of the interface friction angle was not explored, but it could be expected that an increase in the adopted value (25°) would be expected to permit a decrease in the deduced density index of the sand.

The following two Chapters explore the application of the state parameter model through AFENA to the analysis of the soil-structure interaction of a flexible pipe and externally loaded backfill soil. Chapter 7 discusses the applicability of the modelling in two dimensions, while Chapter 8 presents the data from the three-dimensional analyses of the same cases, after discussion of modelling of the pipe in ring compression. The FEA predictions are compared with load-deflection data for the pipes and the loading plate, and earth pressure development within the installations in which pressure cells were employed.

## 6.5 REFERENCES TO THE CHAPTER

Abbo, A. J. and Sloan, S. W. (1995). A Smooth Hyperbolic Approximation to the Mohr-Coulomb Yield Criterion. Computers and Structures, V54, No. 3, pp 427-441.

Carter, J. P. and Balaam, N. P. (1995). AFENA – a General Finite Element Program for Geotechnical Engineeering. School of Civil and Mining Engineering, University of Sydney, Sydney, Australia.

Davis, E. H. (1969). Theories of Plasticity and the Failure of Soil Masses. In "Soil Mechanics, Selected Topics", ed. Lee, I. K., Chapter 6, Butterworths, pp 341-380.

Hardin, B. O. and Black, W. L. (1966). Sand Stiffness under Various Triaxial Stresses. J. Soil Mechanics and Foundation Eng., ASCE, V92, SM2, pp27-42.

Lee, J. and Salgado, R. (2000). Analysis of Calibration Chamber Plate Load Tests. Canadian Geotechnical Journal, V37, pp 14-25.

Naylor, D. J., Pande, G. N., Simpson, B. and Tabb, R. (1981). Finite Elements in Geotechnical Engineering. Pineridge Press, Swansea, Wales, UK.

Tomlinson, M. J. (1975). Foundation Design and Construction. 3rd Edition, Pitman Publishing.

**TABLE 6-I. Values of material constants for the basic single element model**

| Material constants for evaluation of Young's Modulus (eqn. 6-2) | | State Parameter material constants (equation 3-48) | | (eqn. 3-49) | Deformation and strength constants | |
|---|---|---|---|---|---|---|
| **m** | **a** | **$\lambda$** | **$\Gamma$** | **A** | **$\nu$** | **$\phi_c$ (°)** |
| 178 | 0.42 | 0.055 | 1.07 | 0.98 | 0.25 | 31.5 |

**TABLE 6-II. Chosen values of material constants for the refined single element model**

| Material constants for evaluation of bulk modulus, $K_t$ (equation D-2) | | Material constants for evaluation of shear modulus | | | | | Limit on $G_t$ (equation 6-7) |
|---|---|---|---|---|---|---|---|
| | | $G_o$, (equation D-3) | | | $G_t$, (equation D-8) | | |
| **$D_s$** | **$n_k$** | **$C_g$** | **$e_g$** | **$n_g$** | **f** | **g** | **$r_g$** |
| 200 | 0.5 | 300 | 2.3 | 0.5 | 0.99 | 0.2 | 0.03 |

**TABLE 6-III. Summary of FEA analyses to simulate plate-loading test of sand [AFENA, element type 31, Mohr-Coulomb analyses]**

| Run | Side wall fixity | Angle of friction, $\phi$ (°) | Angle of dilation, $\Psi$ (°) |
|---|---|---|---|
| Zero dilation | | | |
| MCR4500 | Rough | 45 | 0 |
| MCS4500 | smooth | 45 | 0 |
| MCR4000 | Rough | 40 | 0 |
| MCS4000 | smooth | 40 | 0 |
| MCR3500 | Rough | 35 | 0 |
| MCS3500 | smooth | 35 | 0 |
| Limited dilation | | | |
| MCR5025 | Rough | 50 | 25 |
| MCS5025 | smooth | 50 | 25 |
| MCR4515 | Rough | 45 | 15 |
| MCS4515 | smooth | 45 | 15 |
| MCR4010 | Rough | 40 | 10 |
| MCS4010 | smooth | 40 | 10 |
| MCR3505 | Rough | 30 | 5 |
| MCS3505 | smooth | 30 | 5 |
| Dilation = angle of friction | | | |
| MCR5050 | Rough | 45 | 45 |
| MCS5050 | smooth | 45 | 45 |
| MCR4545 | Rough | 45 | 45 |
| MCS4545 | smooth | 45 | 45 |
| MCR4040 | Rough | 40 | 40 |
| MCS4040 | smooth | 40 | 40 |

**TABLE 6-IV. Summary of FEA analyses to simulate plate loading test of sand [AFENA, element type 44, State Parameter analyses]**

| Run | Side wall fixity | Density Index of the Sand (%) | No. of increments/10 mm |
|---|---|---|---|
| **Jointed** | | | |
| Saldrum1 | joint | 75 | 2000 |
| Saldrum2 | joint | 50 | 2000 |
| Saldrum3 | joint | 85 | 2000 |
| Saldrum4 | joint | 85 | 5000 |
| Saldrum7 | joint | 85 | 1000 |
| **Non-jointed** | | | |
| Saldrum5 | smooth | 85 | 2000 |
| Saldrum6 | rough | 85 | 2000 |
| Saldrum8 | rough | 65 | 2000 |
| Saldrum9 | rough | 75 | 2000 |

**TABLE 6-V. Values of interface parameters chosen for the FEA of the plate loading test in a sand drum**

| Joint Stiffness (kPa/m) | | Interface Friction Angle (°) | Interface Dilation Angle (°) |
|---|---|---|---|
| Shear Stiffness | Normal Stiffness | | |
| $1.0x10^4$ | $1.0x10^7$ | 25 | 0 |

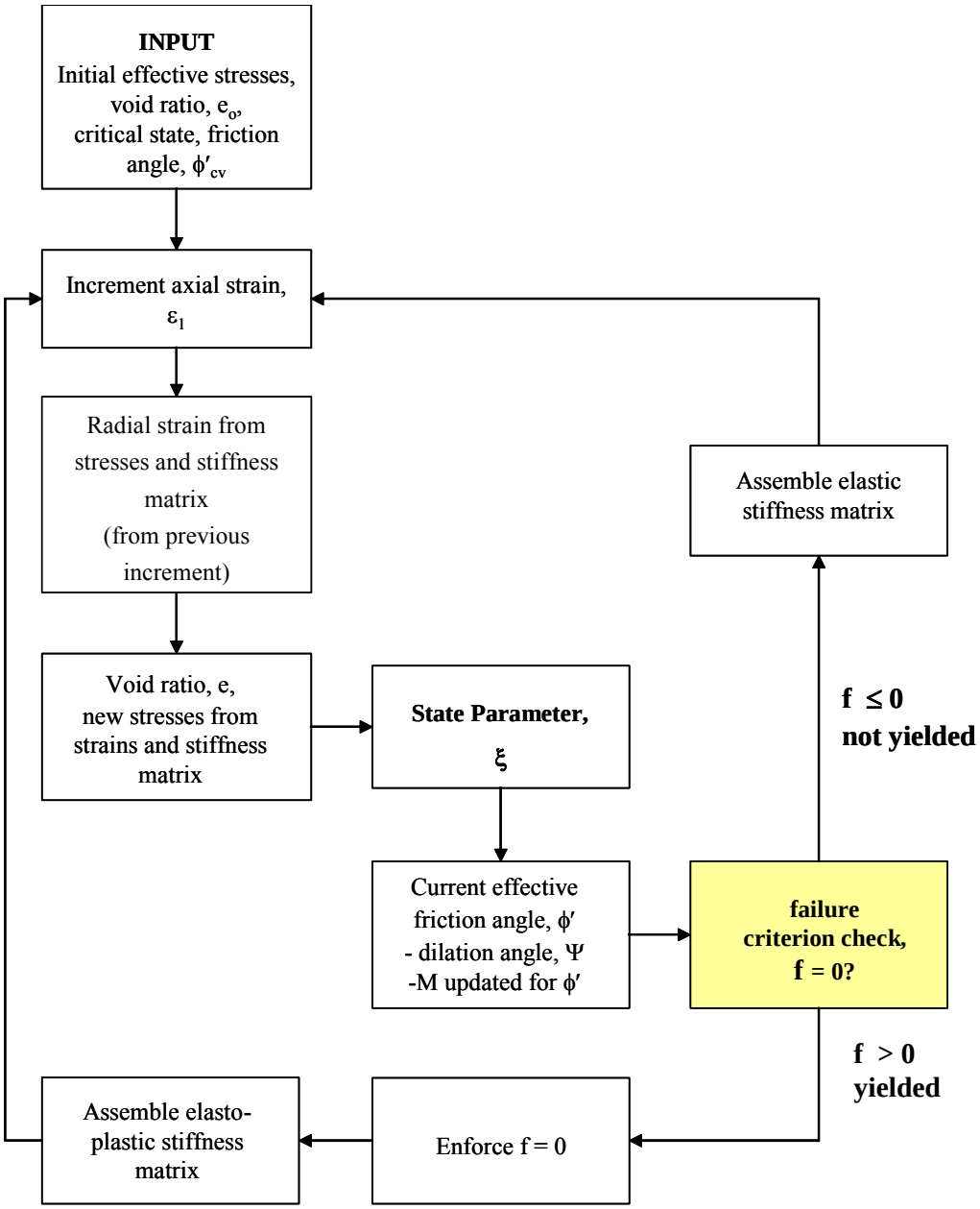


**Figure 6-1. A flowchart for the single element modelling of a conventional triaxial test based on state parameter**

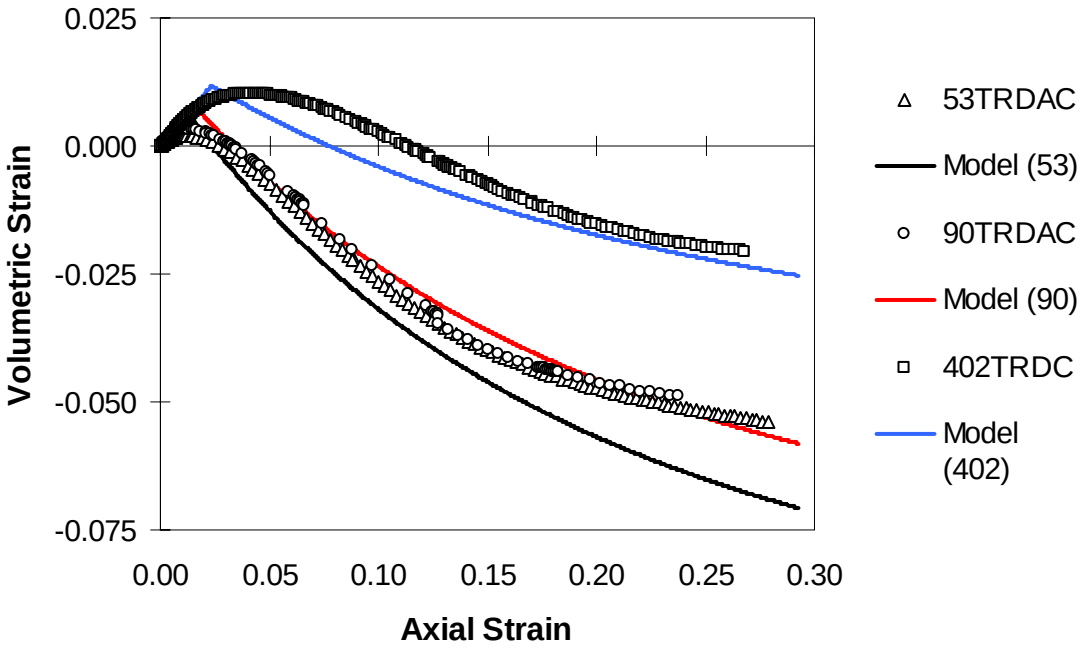


**Figure 6-2 Dilational modelling of the conventional triaxial tests with the initial single element model**

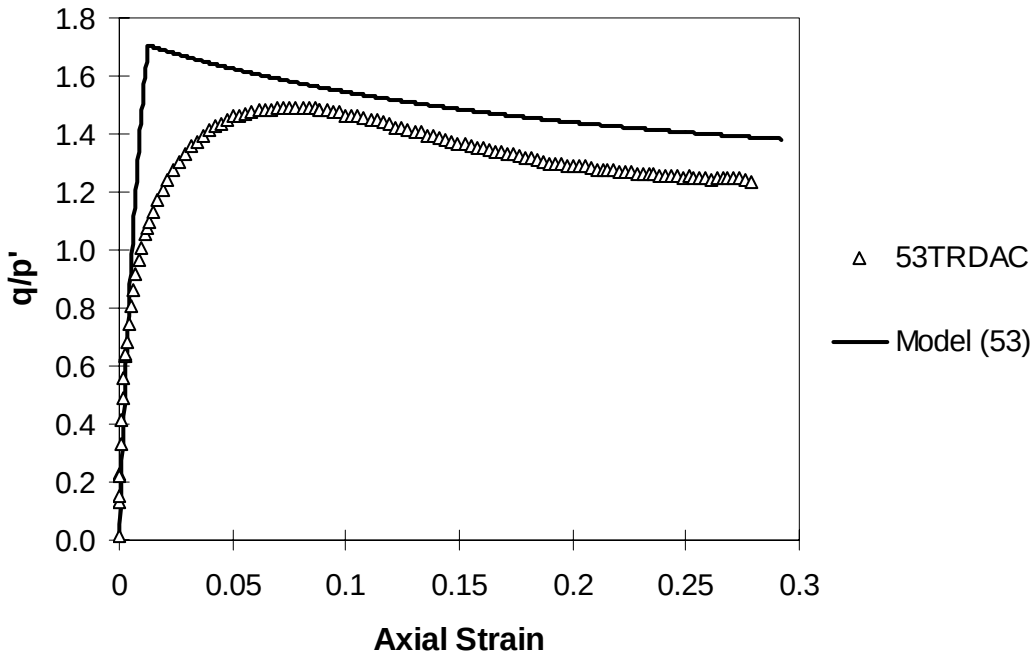


**Figure 6-3 An example of simulation of stress-strain behaviour for a conventional triaxial test with the initial single element model (53TRDAC)**

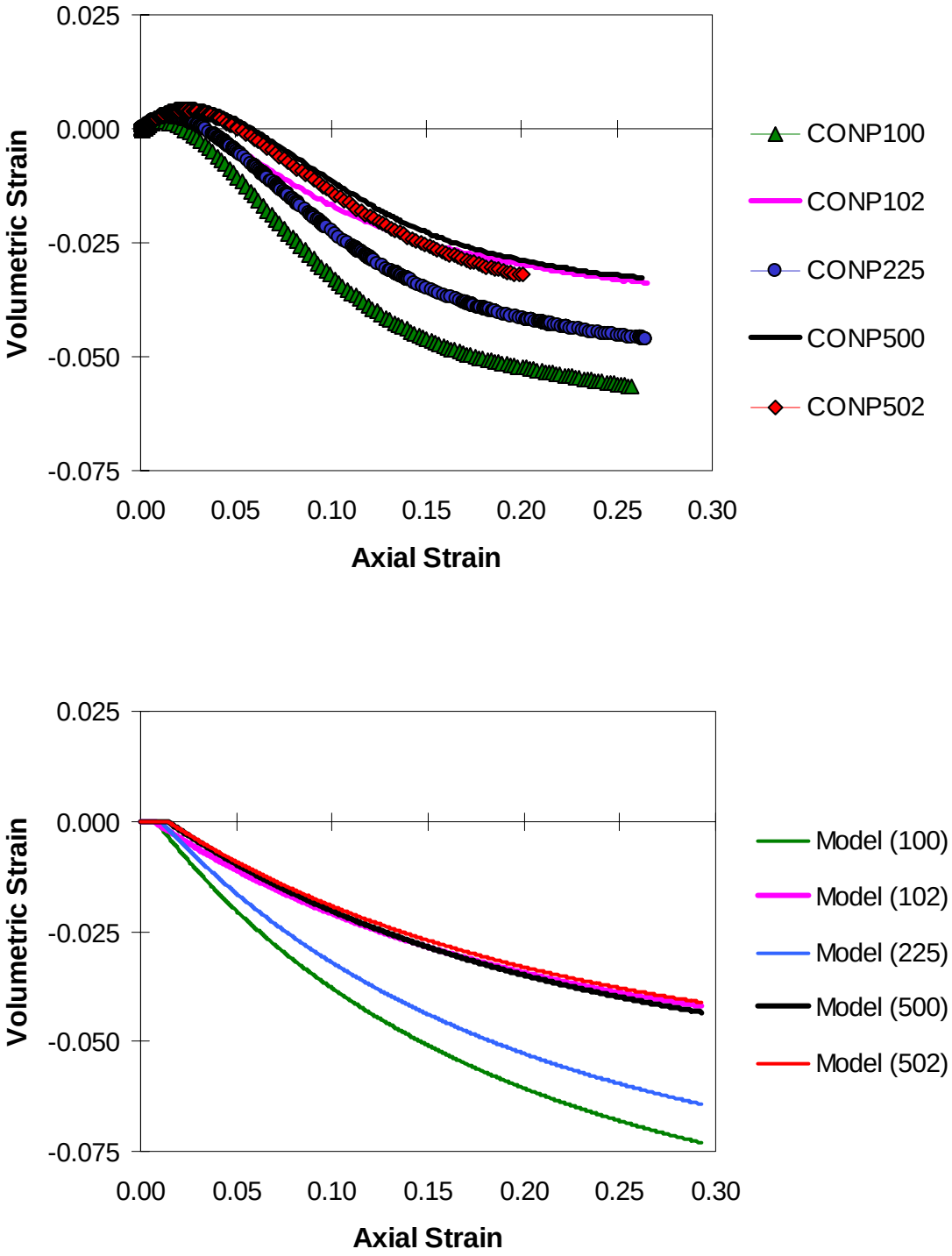


**Figure 6-4 Dilational modelling of the constant mean stress tests with the initial single element model (the top Figure provides the test data while the bottom Figure gives the model predictions)**

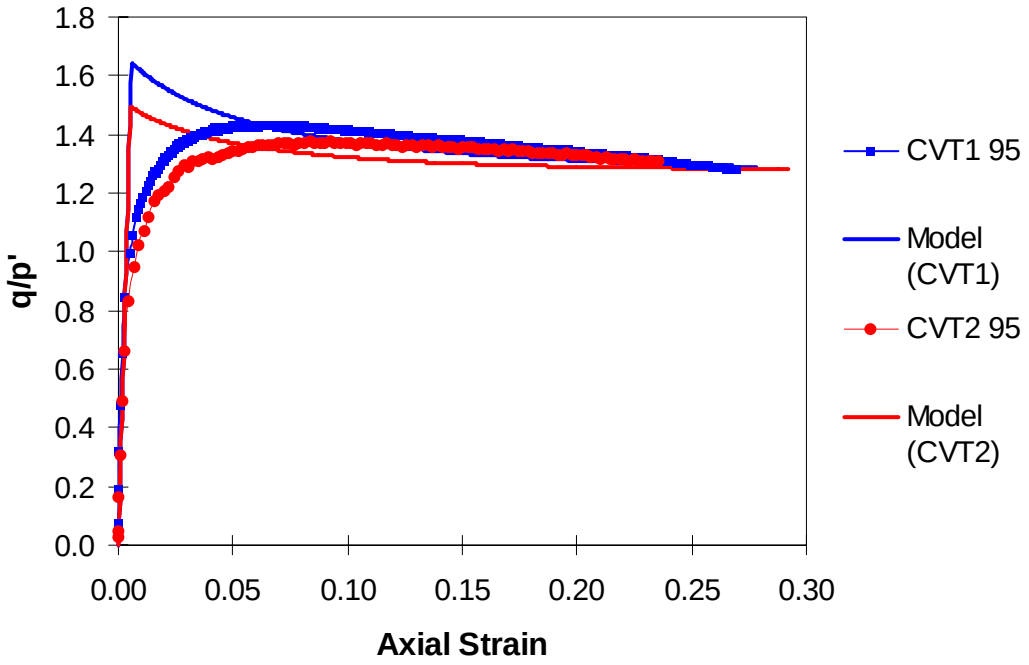


**Figure 6-5 Simulation of stress-strain behaviour for constant volume triaxial tests with the initial single element model (stress ratio against axial strain)**

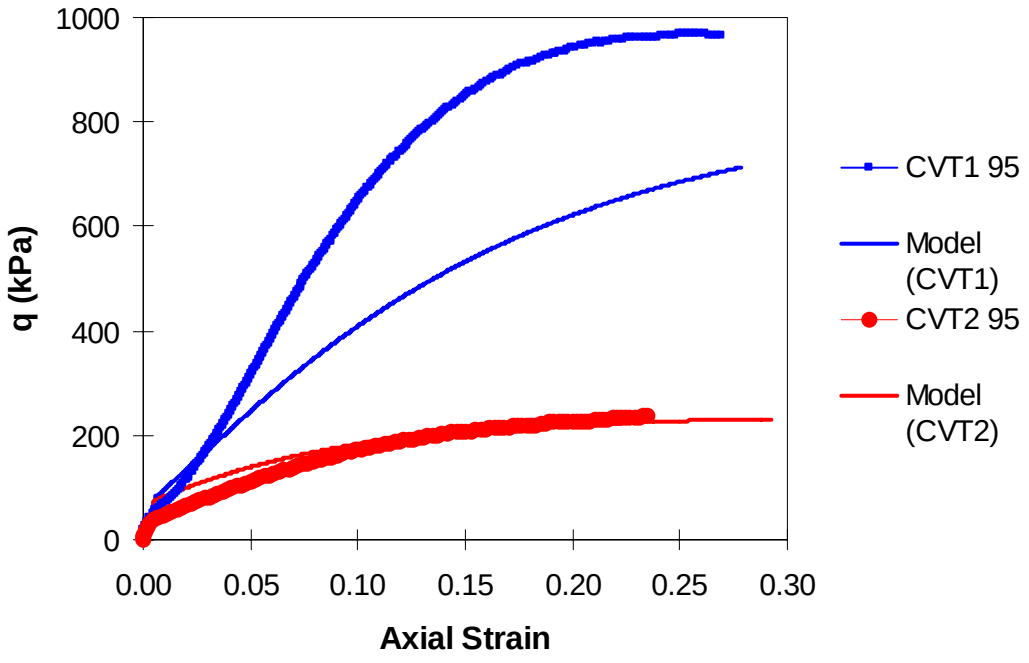


**Figure 6-6 Simulation of stress-strain behaviour for constant volume triaxial tests with the initial single element model**

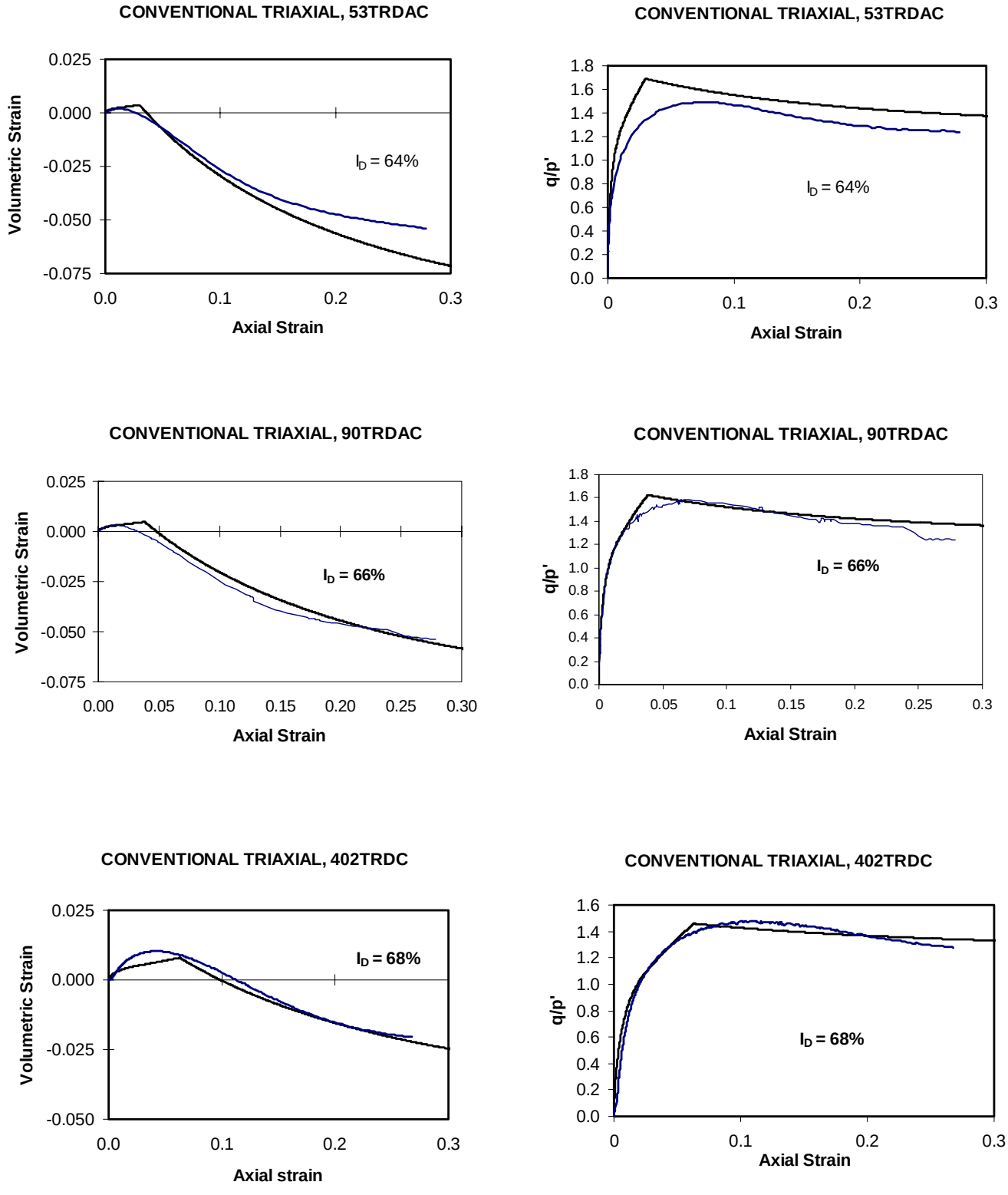


**Figure 6-7. Comparison of single element modelling predictions with data from the conventional triaxial tests using the refined model with set material constants**

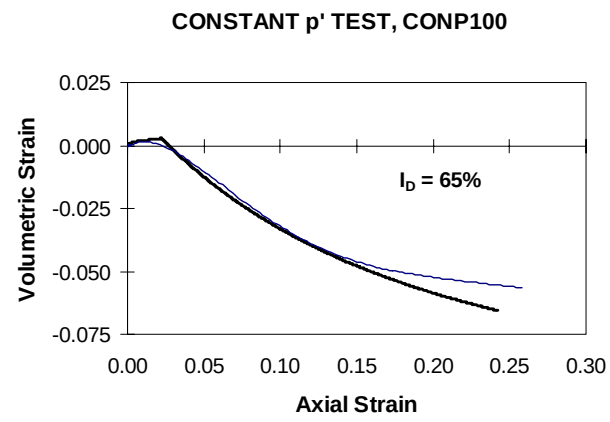


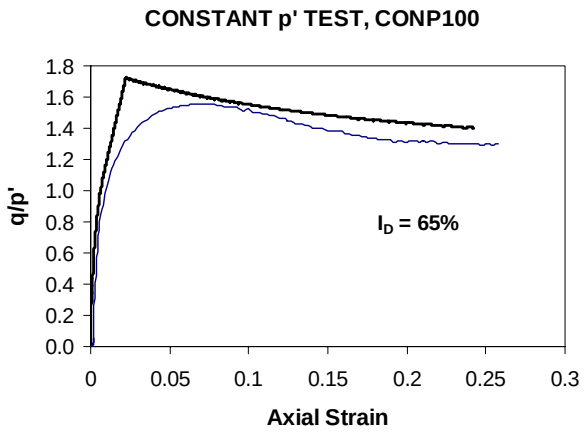


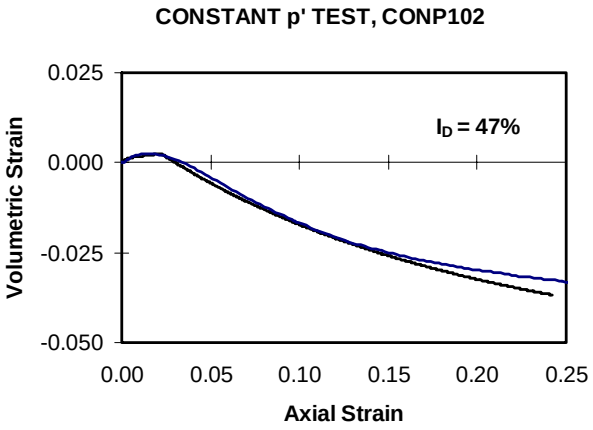


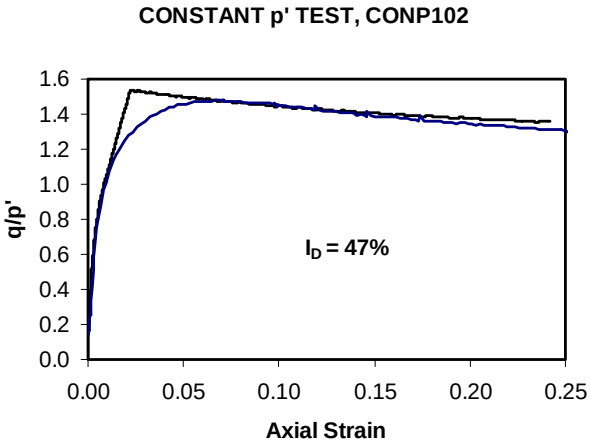


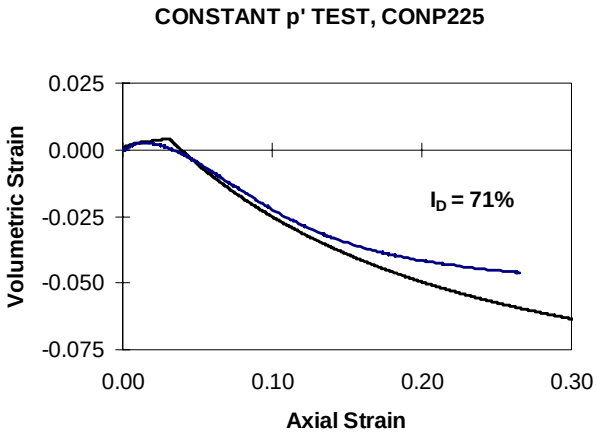


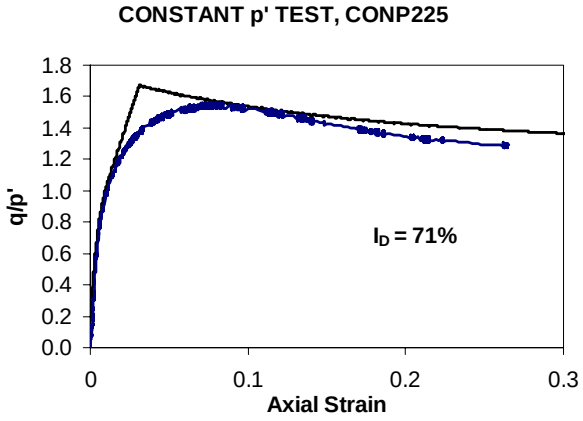


**Figure 6-8. Comparison of single element modelling predictions with data from the constant mean stress tests using the refined model with set material constants (continued over page)**

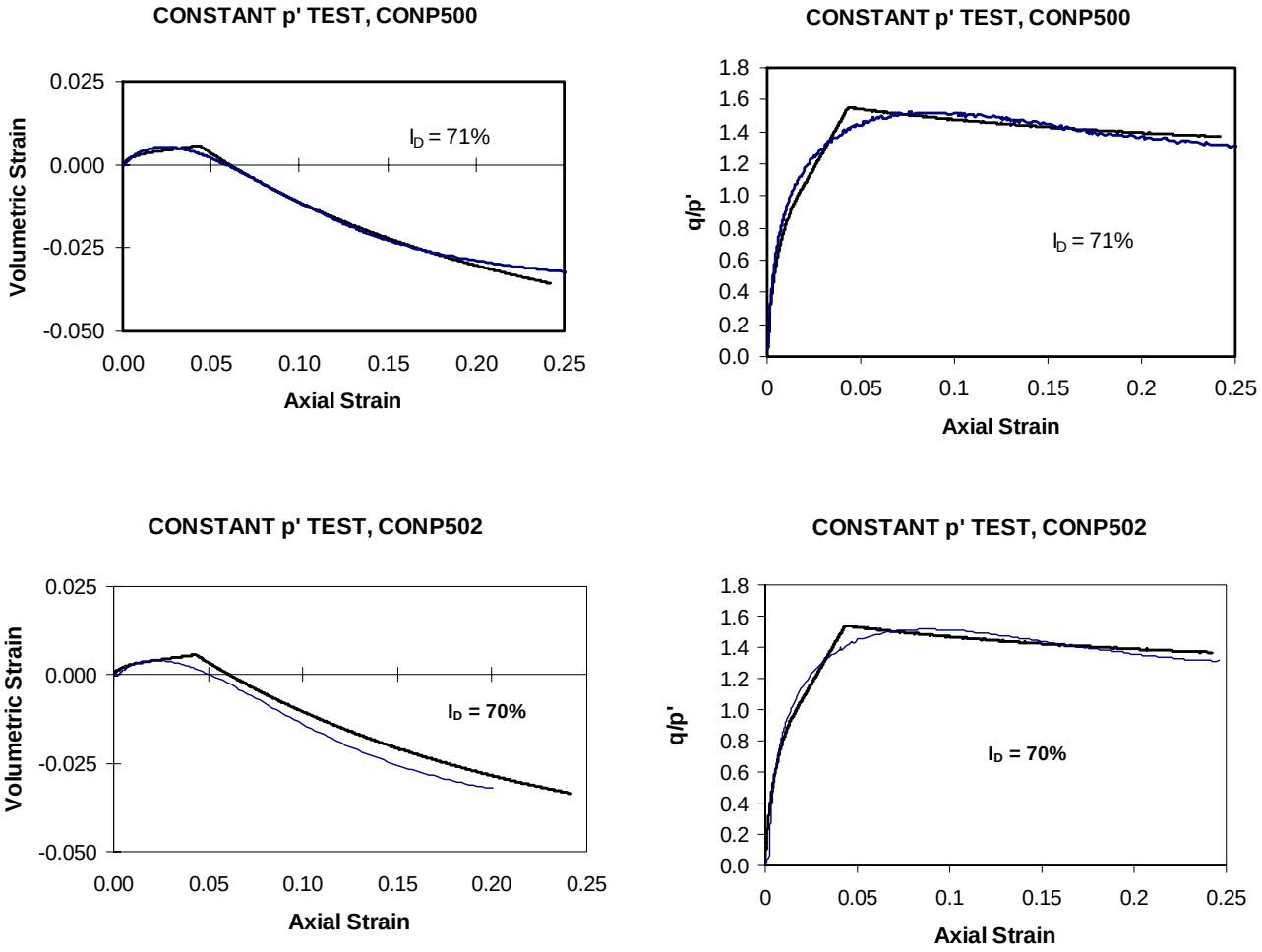


**Figure 6-8 (continued). Comparison of single element modelling predictions with data from the constant mean stress tests using the refined model with set material constants**

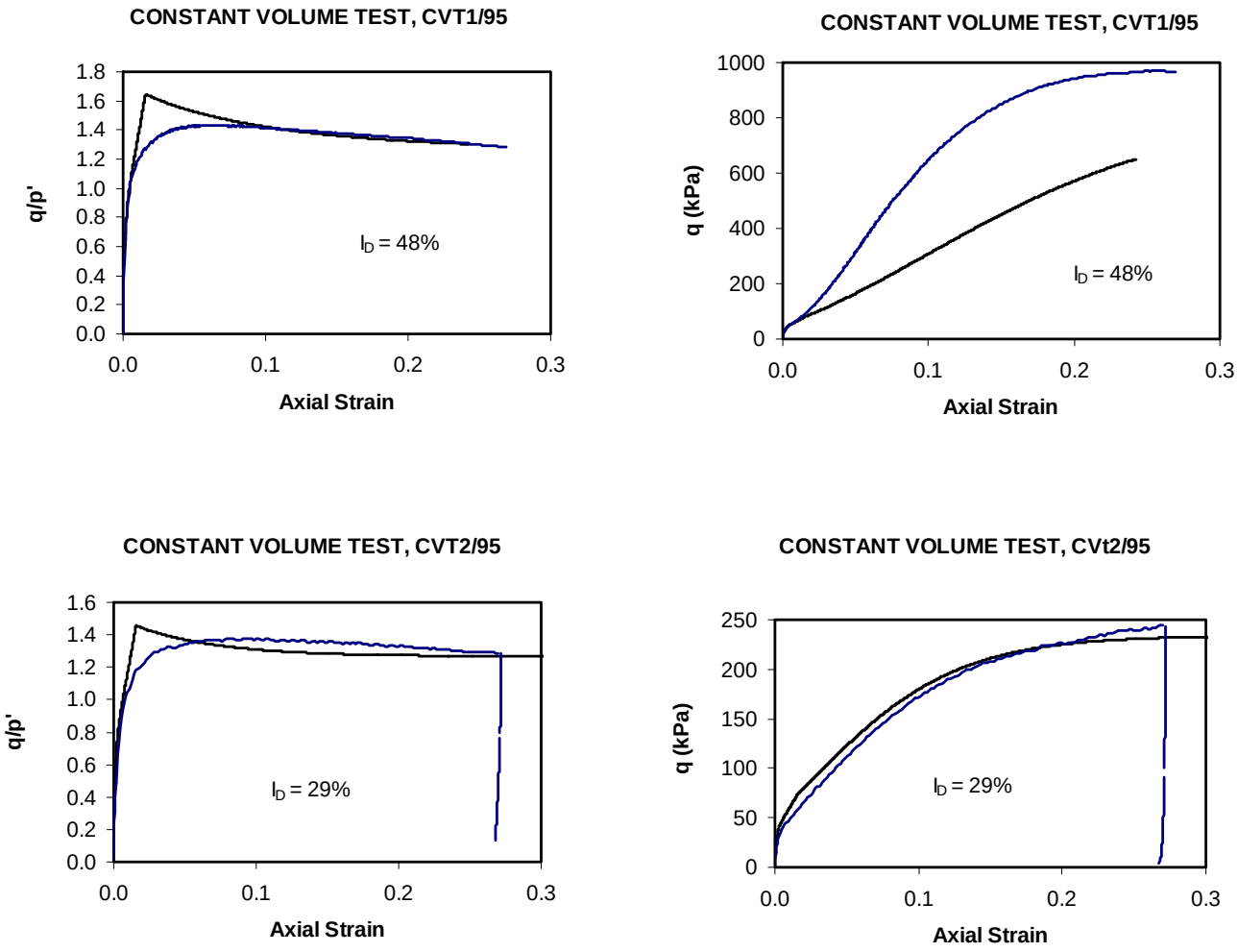


**Figure 6-9. Comparison of single element modelling predictions with data from the constant volume tests using the refined model with set material constants**

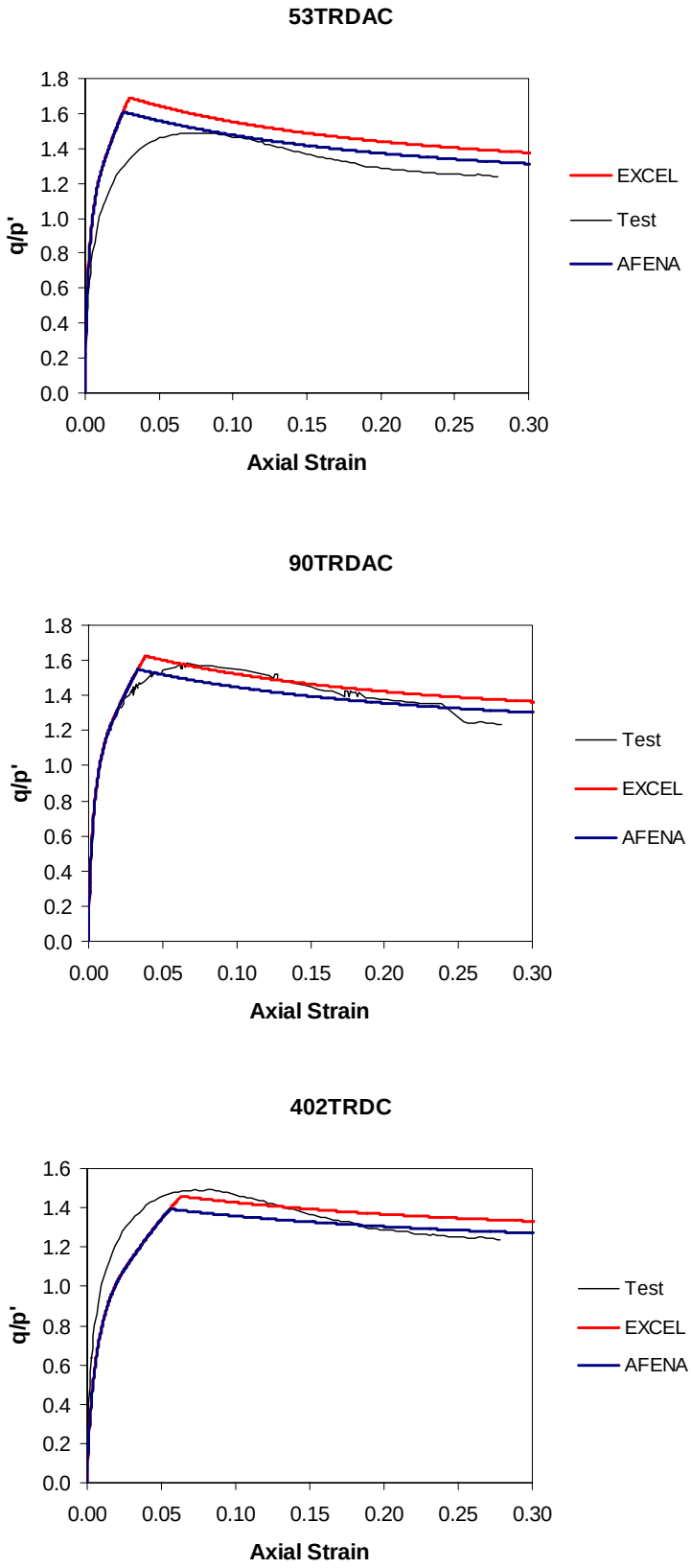


**Figure 6-10. Comparison of the EXCEL® single element model and finite element analysis (AFENA) for the conventional triaxial tests**

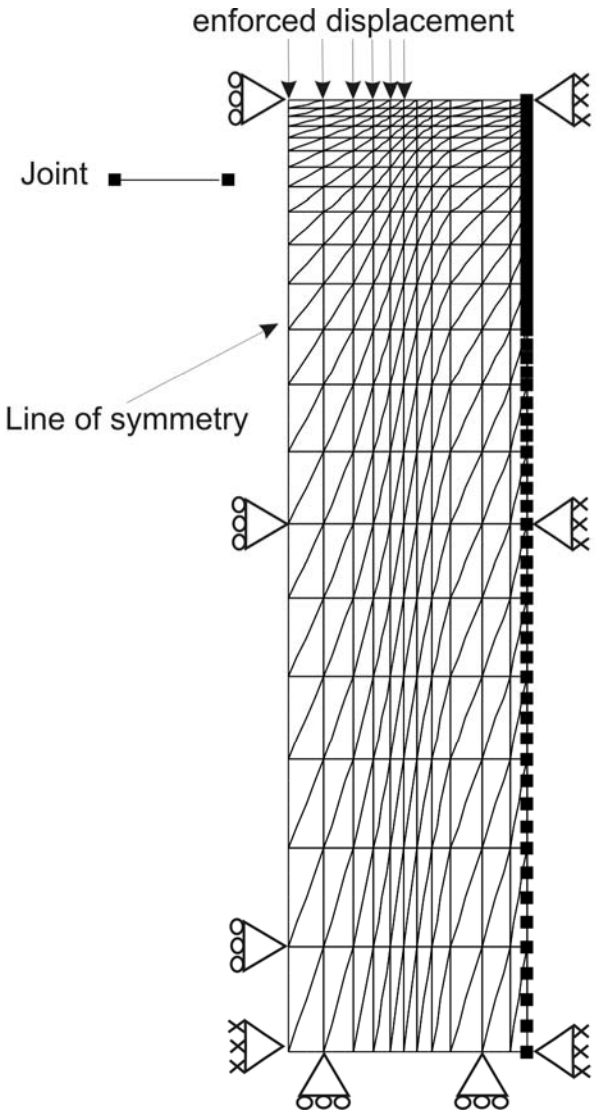


**Figure 6-11. The mesh for FE analysis of the plate loading test (height = 1.15 m, width = 0.2825 m, radius of loaded area = 0.135 m)**

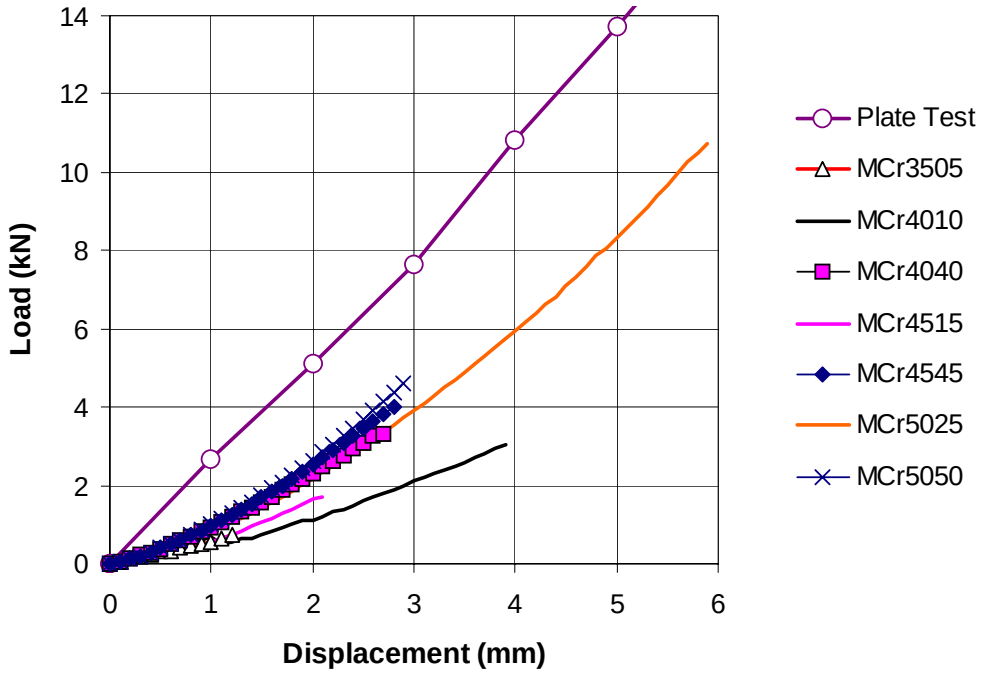


**Figure 6-12. Simulation of plate loading test with Mohr-Coulomb FEA and perfectly rough sidewalls**

**<u>Key to legend</u>: first 2 numerals = ϕ′; next 2 numerals = Ψ, applied in the model**

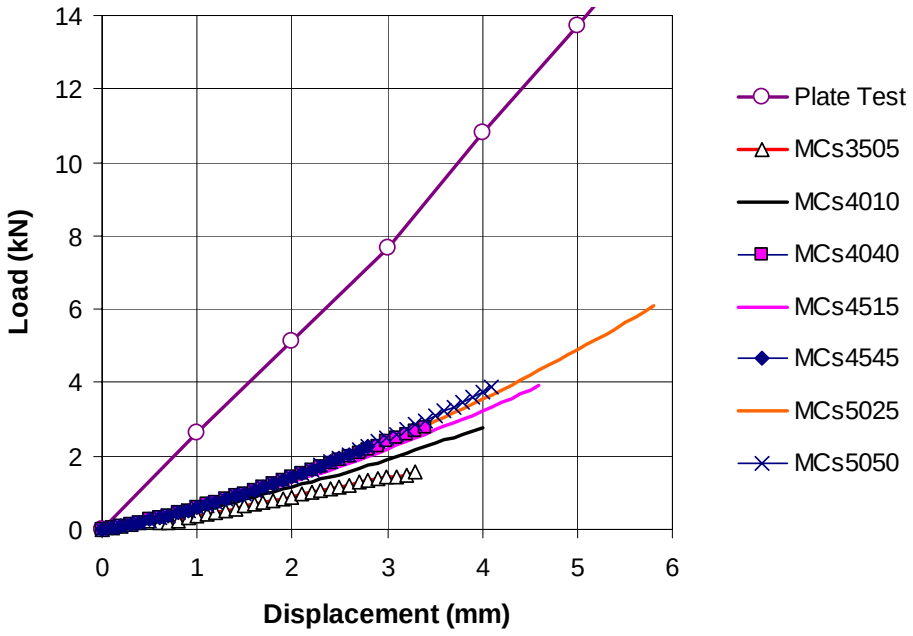


**Figure 6-13. Simulation of plate loading test with Mohr-Coulomb FEA and perfectly smooth sidewalls**

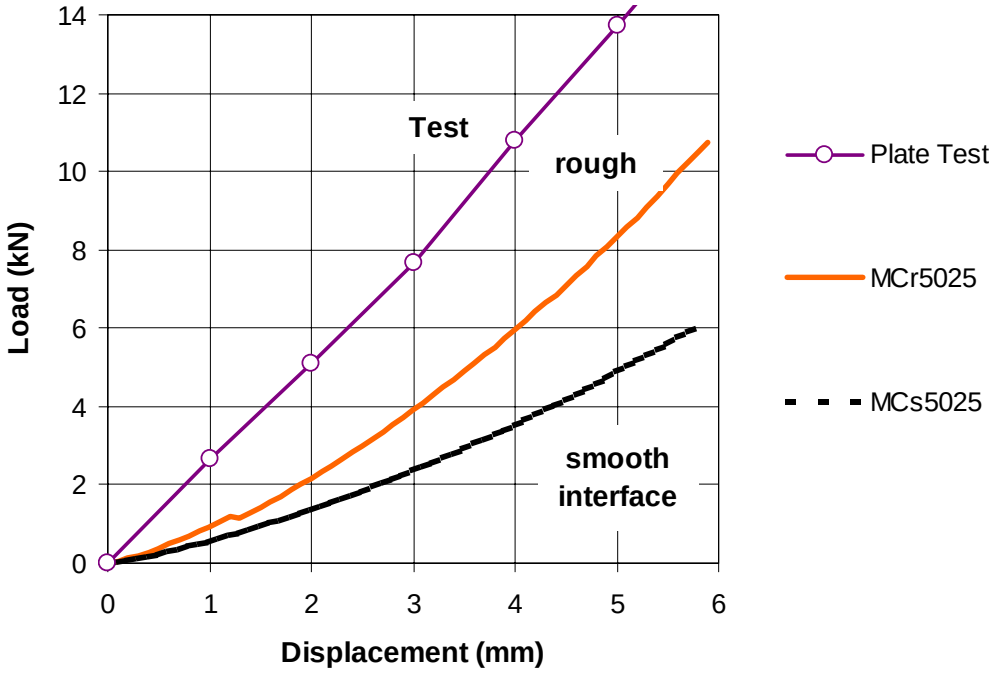


**Figure 6-14. Comparison of Mohr-Coulomb FEA with rough and smooth sidewalls ($\phi' = 50°$ and $\Psi = 25°$)**

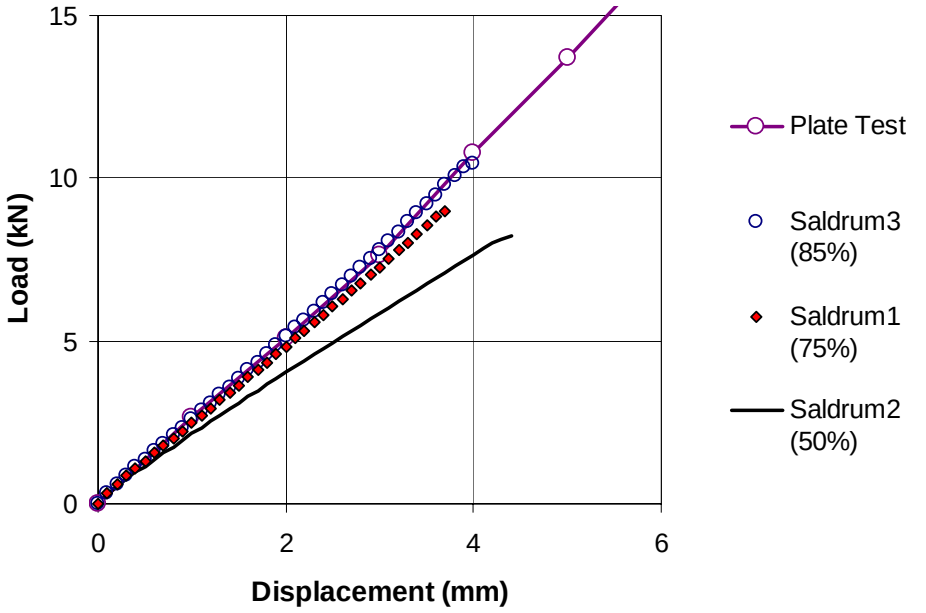


**Figure 6-15. Simulation of plate loading test with State Parameter FEA and interface elements at sidewalls – influence of initial soil density on the solution (density indices are given in the legend in parentheses[1])**

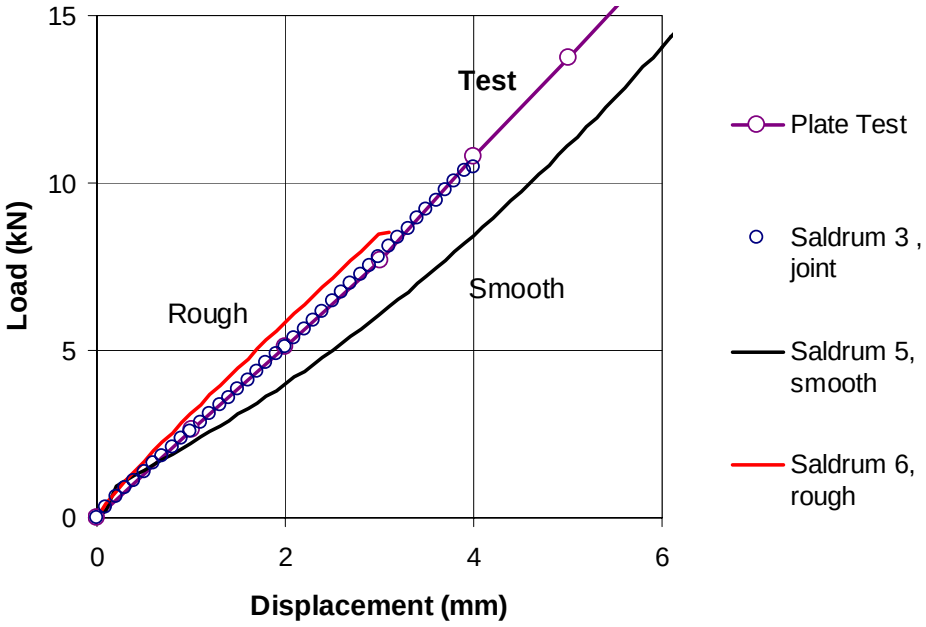


**Figure 6-16. Simulation of plate loading test with State Parameter finite elements – influence of sidewall condition ($I_D$ = 85%)**

[1] The average density index of the sand in the soil box was estimated to be 75%

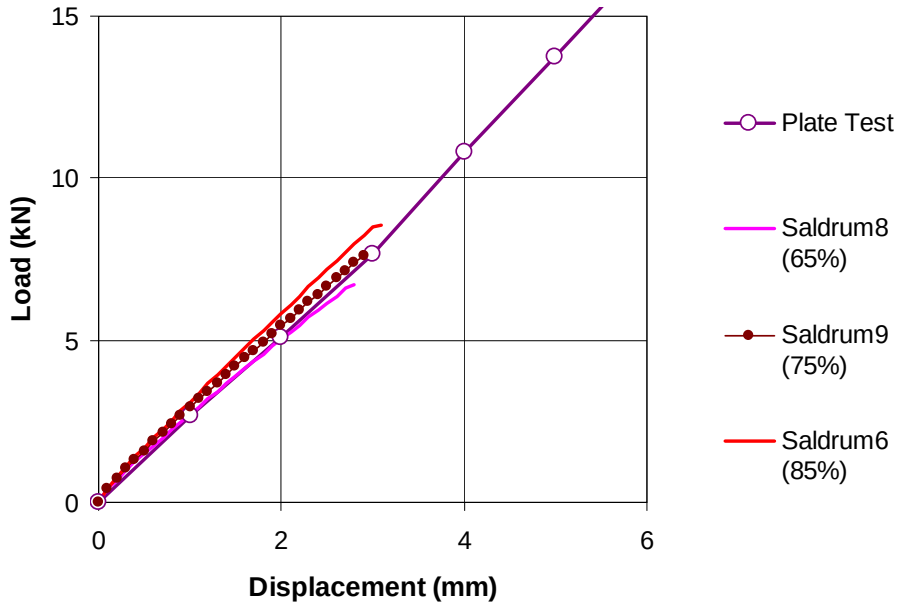


**Figure 6-17. Simulation of plate loading test with State Parameter finite elements and rough sidewall – influence of sand density**

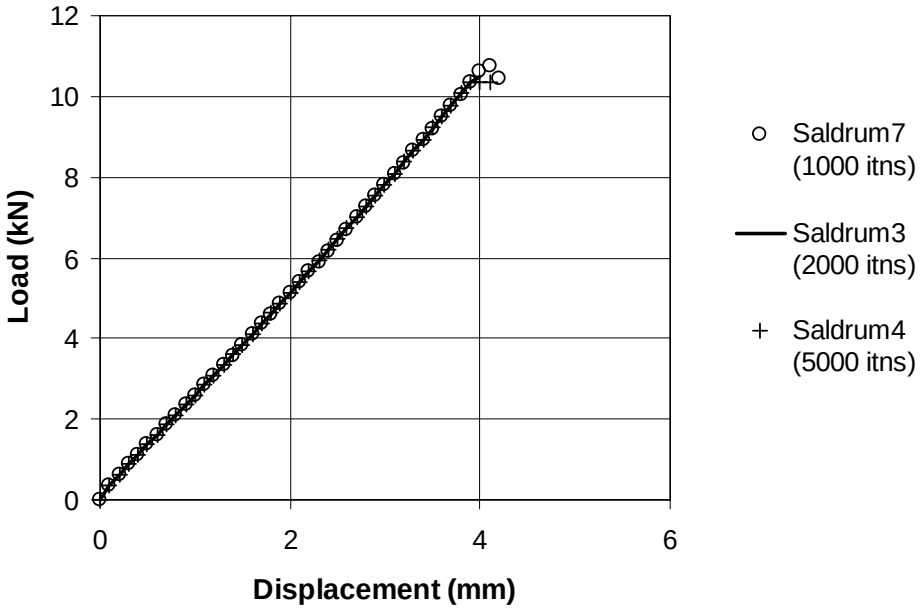


**Figure 6-18. Simulation of plate loading test with State Parameter FEA and interface elements at sidewalls**
**- influence of enforced displacement increment size**

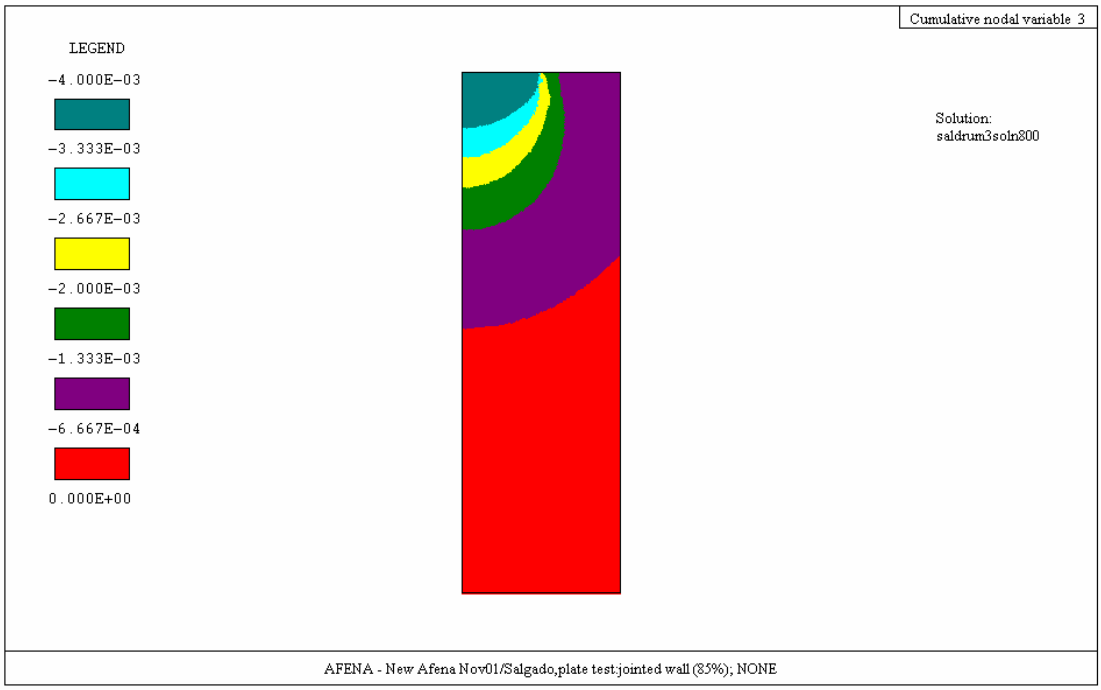


**Figure 6-19. Contour plot of vertical deflections within sand mass: Saldrum3 at 4mm of plate deflection**

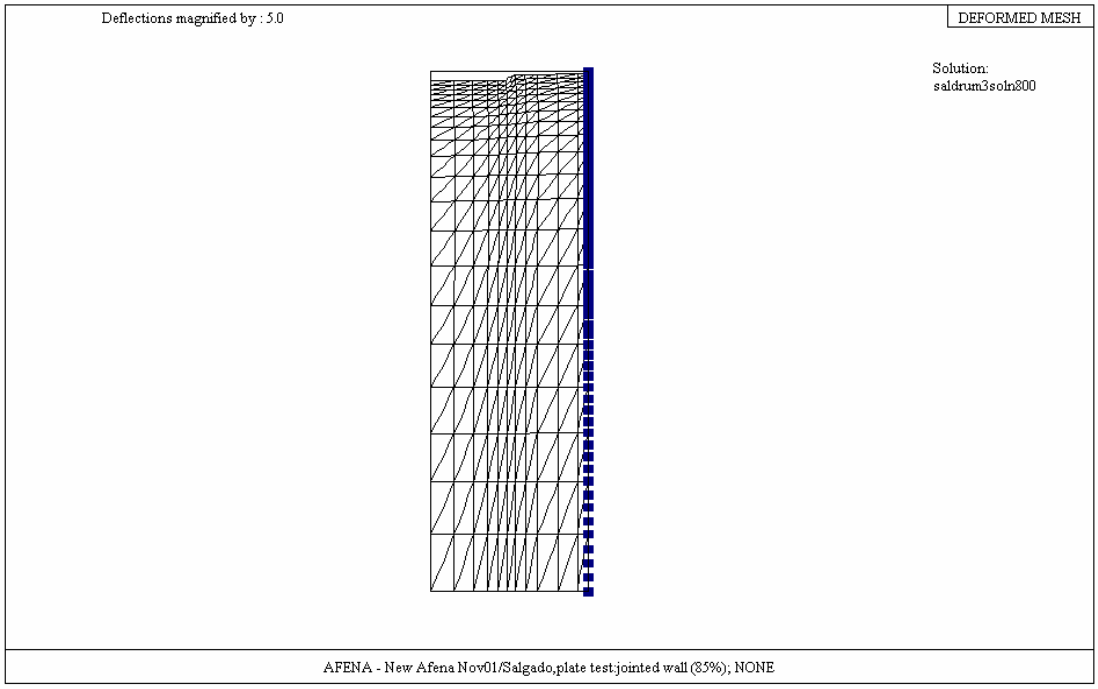


**Figure 6-20. Deformed mesh depicted at a magnification of 5: Saldrum3 at 4mm of plate deflection**

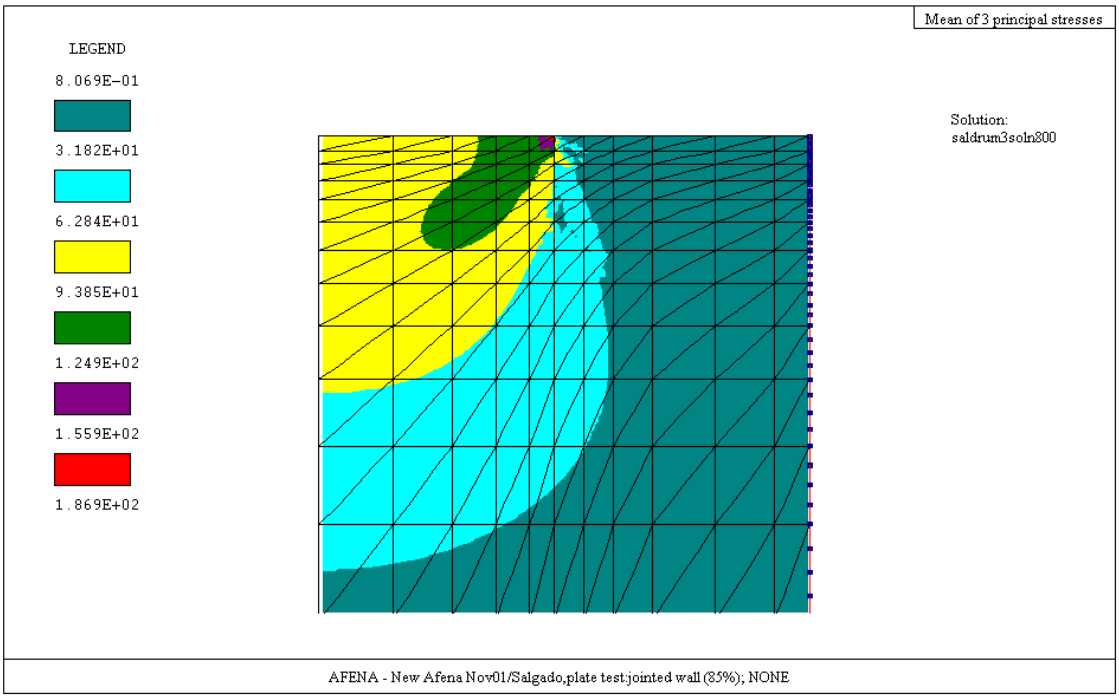


**Figure 6-21. Contour plot of mean effective vertical stress within sand mass: Saldrum3 at 4mm of plate deflection**

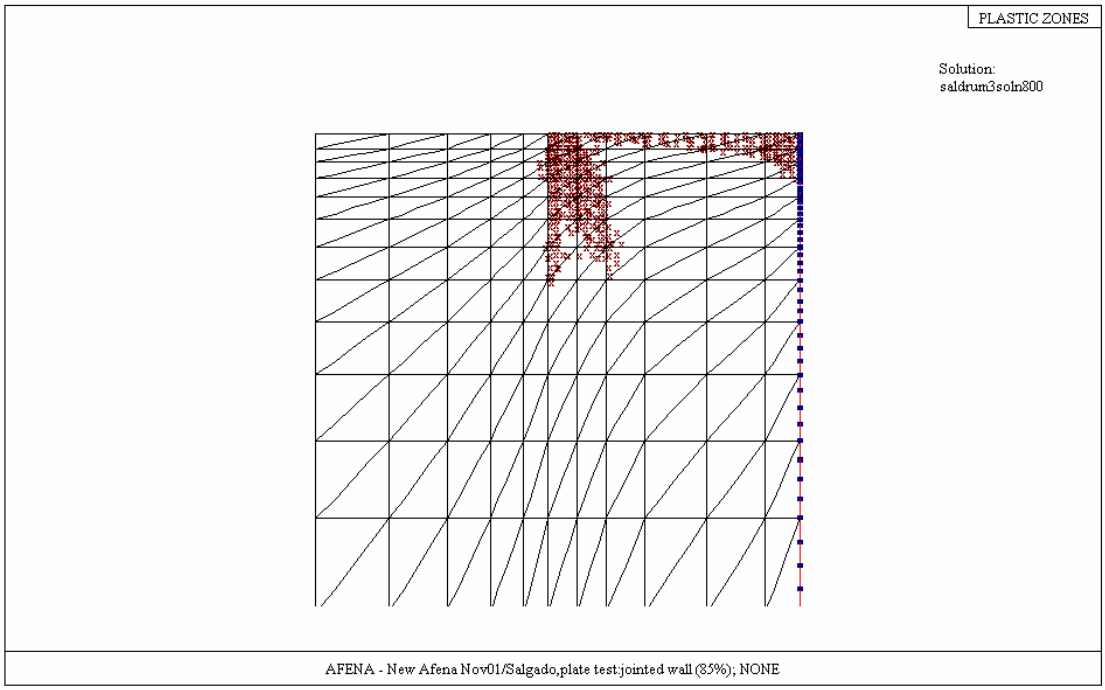


**Figure 6-22. Gauss points which were plastic by 4mm of plate deflection (Saldrum3)**